IEEE Access
Multidisciplinary | Rapid Review | Open Access Journal

Received 12 December 2023, accepted 11 January 2024, date of publication 15 January 2024, date of current version 29 April 2024.

Digital Object Identifier 10.1109/ACCESS.2024.3354383

RESEARCH ARTICLE

Collision Risk Assessment for Intelligent Vehicles Considering Multi-Dimensional Uncertainties

ZHENHAI GAO[1], MINGXI BAO[1], TAISONG CUI[2], FANGYUAN SHI[2], XIANQING CHEN[2], WENHAO WEN[1], FEI GAO[1], AND RUI ZHAO[1], (Member, IEEE)

[1]State Key Laboratory of Automotive Simulation and Control, Jilin University, Changchun 130022, China
[2]Chongqing Chang'an Automobile Company Ltd., Chongqing 400023, China

Corresponding author: Rui Zhao (rzhao@jlu.edu.cn)

This work was supported by the National Science Foundation of China under Grant 52202494 and Grant 52202495.

ABSTRACT To ensure the reliability of autonomous driving, the system must be capable of potential hazard identification and appropriate response to prevent accidents. This involves the prediction of possible developments in traffic situations and an evaluation of the potential danger of future scenarios. Precise Collision Risk Assessment (CRA) faces complex challenges due to uncertainties inherent in vehicle and road environmental conditions. This paper introduces a new CRA approach, the Multi-Dimensional Uncertainties-CRA (MDU-CRA), which integrates uncertainties related to driver behavior, sensor perception, motion prediction models, and road infrastructure into a comprehensive risk evaluation framework. The estimation of vehicle state is initiated using Extended Kalman Filtering (EKF) to capture uncertainties in sensor perception. Concurrently, a probabilistic motion prediction model based on Gaussian distributions has been developed, which considers the uncertainty in driver behavior. Subsequently, the uncertainty of the road structure is modeled using a truncated Gaussian distribution. Finally, collision risk is quantified as the future probability of collision through heuristic Monte Carlo (MC) sampling. This paper presents the results of two experiments Firstly, our proposed method is demonstrated to outperform the reference neural network-based method in terms of short-term motion prediction accuracy. Secondly, two driving scenarios are extracted and reconstructed from the Next Generation Simulation (NGSIM) dataset for validation and evaluation, i.e., an active lane-change scenario and an emergency braking scenario. In the domain of collision risk assessment, our approach consistently outperforms other evaluation methods. It exhibits the capability to perceive collision risks 2 to 5 seconds in advance, significantly reducing the probability of imminent collision incidents.

INDEX TERMS Motion prediction, collision risk assessment, intelligent vehicles, multi-dimensional uncertainties.

I. INTRODUCTION

Safety stands as the foundational pillar for both Advanced Driver Assistance Systems and Autonomous Vehicles [1]. A major challenge lies in the real-time detection of dangerous situations and the initiation of responses to prevent accidents [2]. Central to this challenge is the need for accurate short-term risk assessment, which involves the prediction of future collision probabilities by forecasting the evolution of the current traffic situation of surrounding vehicles.

Presently, risk prediction methodologies bifurcate into two streams: deterministic and probabilistic, distinguished by their consideration of future motion uncertainties. The deterministic variant typically relies on physics-driven motion models [3], [4], [5], [6], [7], [8], [9], such as constant velocity (CV), constant acceleration (CA), and constant yaw rate and acceleration (CYRA). These models predict vehicular trajectories and subsequently compute risk metrics like Time-to-Collision (TTC) [3], Time-to-Brake (TTB) [4], and

The associate editor coordinating the review of this manuscript and approving it for publication was Wei Wei.

Time-to-Steer (TTS) [5]. This schema extends to the identification of potential trajectory intersections [6], [7], [8] or analysis of intersection duration across a given trajectory [9], [10], [11]. However, a deterministic paradigm has intrinsic limitations, as it fails to capture future motion uncertainties or factor in the influence of road geometry on vehicular trajectories [12]. Consequently, in the context of collision predictions, it is crucial to acknowledge the possibility of unanticipated risk factors arising from deviations in human or autonomous driving system behavior from expected inputs. Additionally, the fidelity of risk assessments may be compromised if the state estimation by the perception system is biased, particularly in edge cases. Furthermore, discrepancies between the kinematic model's projections of reachable areas and the actual road geometry can result in an underestimation of risks.

To address maneuver-intention-related limitations, a method centered on maneuver-oriented trajectory prediction has emerged. This approach begins with the deduction of a driving maneuver, followed by the generation of trajectories aligned with these identified maneuvers. The assessment of vehicular maneuvers pivots on the compatibility between ongoing vehicle movements and the overarching road infrastructure, including lane configurations and driving lanes [13]. Additionally, probabilistic analysis methods, encompassing the Hidden Markov Model (HMM) [14], Dynamic Bayesian Networks (DBN) [15], [16], and a combination of Artificial Neural Network (ANN) with Support Vector Machine (SVM) [17], prove viable for intention recognition through observational sequences or dataset training. Considerable progress has also been made in intention recognition through machine learning techniques [18] or game theory [19]. When combined with maneuver intents, data-centric deep learning architectures [20], [21] such as Long Short-Time Memory (LSTM) networks [22], [23], [24] and graph convolution networks (GCN) [25] take precedence over other methods. Moreover, deterministic quantitative indicators are employed to evaluate the collision risk between vehicular trajectories. While this model has demonstrated promising results in long-term trajectory prediction, its generalization capability is constrained due to the lack of training datasets for intricate urban scenarios. Additionally, the method's assessment of collision risk does not adequately account for uncertainty information.

Similar to the deterministic method, MC offer an alternative approach as it generates potential future trajectories through random control inputs. Subsequently, they estimate collision probabilities by counting the number of trajectories resulting in collisions [11], [26]. However, conventional MC simulations usually rely on deterministic models and fail to capture essential uncertainties. Therefore, their prediction accuracy degrades in dynamic situations, such as emergency braking or complex road layouts.

A probabilistic approach presents another methodology for risk evaluations, considering motion uncertainty. This technique incorporates error propagation along the predicted trajectory, indicating the ambiguity of future states [27], [28]. Typically, uncertainty is modeled using the Kalman filter, which assumes a Gaussian distribution of future vehicle positions [3], [29], [30], [31]. Additionally, collision probabilities are calculated based on the overlap of ellipsoids representing vehicle state variance [29]. MC simulations are frequently utilized to calculate the collision probability based on the joint Gaussian distribution [26], [27]. Nonetheless, the motion uncertainty, characterized by the Gaussian distribution, neglects road geometry and driver behaviors (control input), inadequately representing uncertainties observed in real-world driving scenarios.

Therefore, to address the aforementioned challenges, we introduce in this paper the Multi-Dimensional Uncertainties Collision Risk Assessment (MDU-CRA) method, specifically designed for accurate assessment of short-term collision risks. This is achieved by a multi-dimensional, uncertainty-aware probabilistic motion prediction for both the ego vehicle and its neighboring traffic. Distinct from prevailing prediction strategies rooted in Gaussian distribution, our proposed method models future motion uncertainty by considering the uncertainties in sensor perception, driver behavior, motion prediction model, and road structure. As a result, it is better equipped to articulate motion uncertainties found prevalent in real-world driving scenarios. The main contributions of this paper are summarized as follows:

(1) Firstly, we present a computational method for driver behavior and utilize an EKF is utilized to emulate the uncertainty in sensor perception. Moreover, we have developed a Gaussian distribution-based motion prediction model that incorporates the intrinsic uncertainties of driver behavior, sensor perception and motion prediction model.

(2) Secondly, to simulate uncertainties in the road environment, we harness the truncated Gaussian distribution to enable sampling within a confined region. With heuristic MC sampling conducted from the Gaussian distribution of potential future trajectories, we assess the collision between each possible pair to quantify collision risk in terms of the probability of future collisions.

(3) Thirdly, to enhance the practicality of the algorithm and reduce the complexity of the computational model, we introduce a distance-based deterministic collision detection algorithm, which means that in areas deemed absolutely safe or dangerous, the current probability is determined directly without the need for complex MC sampling.

(4) Fourthly, we conduct two experiments to validate the effectiveness of our proposed method. The results illustrate that our method outperforms the referenced neural network-based method in terms of short-term motion prediction accuracy and accurately assesses collision risk.

The remaining sections of this paper are organized as follows. Section II introduces our framework and system architecture. Section III illustrates the multi-dimensional uncertainty probability motion prediction. Section IV

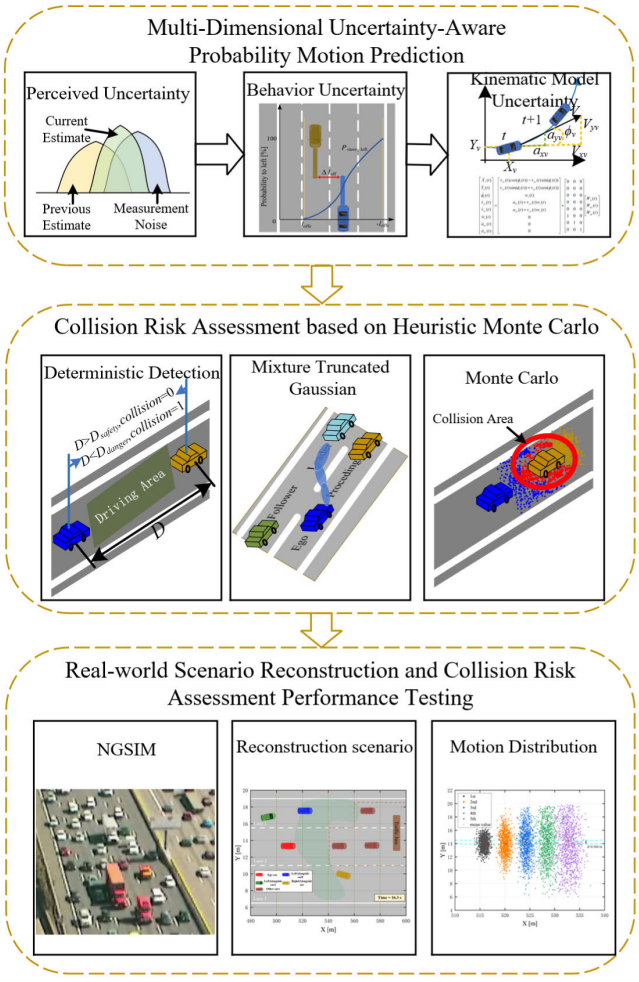

FIGURE 1. The overall framework of proposed collision risk assessment.

describes the CRA employing a heuristic MC approach rooted in the truncated Gaussian distribution. Furthermore, Section V details the experimental settings and presents the results. Finally, the conclusions and future work are summarized in Section VI.

II. FRAMEWORK OF MDU-CRA

The overall framework of the proposed multi-dimensional uncertainties collision risk assessment approach for intelligent vehicles is depicted in Fig. 1. The blue vehicle represents the controlled ego vehicle (denoted as *ego*), while various object vehicles, such as preceding, leaders, and followers, are represented with distinct color designations. This method allows for a nuanced understanding of vehicular interactions in complex traffic scenarios, enriching the adaptability and predictive capabilities of our model.

Firstly, we introduce a probabilistic motion prediction model that considers multi-dimensional uncertainties. A driver model is developed to encompass uncertainties in human driving behaviors, complemented by the use of Extended Kalman Filtering (EKF) to mitigate uncertainties from sensor measurements. Simultaneously, kinematic models that integrate perceptual data from the driving environment are formulated for the ego vehicle (CYRA) and other object vehicles (CV). These models account for variances in driver behavior (as discussed in section III-B), sensor perception (as described in section III-C), and the motion prediction model (as detailed in section III-D) and ensure a comprehensive understanding of vehicle trajectory uncertainties in future scenarios.

Next, we propose a collision risk assessment algorithm that accurately estimates the risk of collisions within a specified time frame. This is achieved by a probabilistic vehicle motion prediction model and heuristic MC methods. Absolute danger and safety scenarios are identified through deterministic detection based on the location of vehicles. This approach eliminates the necessity for MC sampling in situations where hazardous or safe conditions are clearly defined, thereby enhancing the efficiency of MDU-CRA. Collision probabilities are directly inferred by the system when deterministic thresholds are satisfied. In instances where the mean distance of future positions between the ego and object vehicle falls within the danger and safety thresholds, sampling is conducted using MC methods based on truncated Gaussian distribution. This distribution, truncated in accordance with road edges, prevents sampling in locations inaccessible to vehicles, incorporating uncertainties in road structure. Consequently, this method enhances assessment efficiency and accuracy.

Finally, to validate our approach, we conducted an analysis on two driving scenarios derived from the NGSIM Dataset: the active lane-change scenario and the emergency braking scenario. Comparative evaluations emphasize the advantages of our approach over conventional collision detection methodologies, highlighting its capacity to predict potential collisions with an extended lead time. This provides drivers with more time to react and avoid impending dangers.

III. MULTI-DIMENSIONAL UNCERTAINTY-AWARE PROBABILITY MOTION PREDICTION

An integrated approach for capturing motion uncertainties is presented in this section. Specifically, uncertainties related to sensor measurements are modeled using EKF. Additionally, a probabilistic motion prediction model is developed, which explicitly incorporates uncertainties associated with driver behaviors. By harmonizing these methods, short-term motion forecasting is achieved for both the ego vehicle and its surrounding vehicles, thereby constructing a comprehensive and robust predictive model for complex traffic scenarios.

A. EGO AND OBJECT VEHICLE MODELS

It is posited that for a comprehensive understanding of the vehicle's surroundings, the vehicle is equipped with advanced on-board sensing systems, notably lidar and camera. Such a system not only empowers the ego vehicle to actively perceive the environment but also to record historical vehicle positions. The configuration representing the vehicle is succinctly

captured in (1).

$$\begin{cases} X_v = [x_v, y_v, \phi_v, v_{xv}, v_{yv}, \omega_v, a_{xv}, a_{yv}]^T \\ X_o = [x_o, y_o, v_{xo}, v_{yo}, a_{xo}, a_{yo}]^T \end{cases} \tag{1}$$

where, X_v, X_o represent the configurations of the ego and object vehicle, respectively. (x_v, y_v) denote the coordinates of the ego vehicle at the current time. Its heading angle is given by ϕ_v. (v_{xv}, v_{yv}) indicate the velocities along the x and y axes. ω_v is yaw angular velocity and (a_{xv}, a_{yv}) refer to the angular velocities along the x and y axes. For the object agent, (x_o, y_o) depict its current coordinates. Its velocities on the x and y axes are represented by (v_{xo}, v_{yo}), while (a_{xo}, a_{yo}) denote its angular velocities on those axes. All variables are defined in the reference frame of the ego vehicle.

B. DRIVER BEHAVIOR UNCERTAINTY MODELING

In the intricate landscape of microscopic traffic flows, the ego vehicle frequently engages in complex behavioral interactions with surrounding object vehicles. These interactions can manifest as car-following, lane-changing, and merging behaviors, among others. In potentially dangerous scenarios, the certainty of a collision between the ego and object vehicle is rendered ambiguous due to the intervention of the driver, who often takes preemptive action to mitigate imminent collisions. The choice of response—be it steering adjustments, braking, variations in input magnitude or direction, or other evasive maneuvers—is inherently uncertain and deeply rooted in the variability of individual driver behaviors. Recognizing this element of unpredictability, this work incorporates the dimension of driver behavior uncertainty into the MDU-CRA.

Drawing from real-world scenario statistics, a three-tiered driver maneuver model is formulated, subsequently leading to the genesis of a multi-level risk situation. Table 1 delineates the range of steering and braking inputs for each risk situation level, contingent upon the perceived threat level from the surrounding vehicular environment. Drivers evaluate their actions based on the surrounding environmental context, primarily focusing on the relative distance between vehicles. In the first driver model, when the distance between vehicles exceeds $D_{\text{level\_1}}$, there's ample space for the driver to maneuver and avoid collisions. Typically, drivers resort to braking inputs to mitigate imminent threats, ensuring a safety buffer between their own vehicle and any obstructing vehicle, thus resulting in a level-1 risk situation. This model mirrors a commonly observed driving behavior, boasting universal applicability. The second driver model is invoked when the conditions of a level-1 risk situation aren't met, i.e., the relative distance falls between $D_{\text{level\_1}}$ and $D_{\text{level\_2}}$. This model integrates both steering and braking inputs to further prevent collisions. Steering adjustments, frequently employed by drivers, are either to adapt to unsatisfactory driving conditions or to secure more driving space, manifesting as lane changes or collision avoidance. For this model, the average steering and braking inputs lie at 0.2 g with a standard deviation of 0.05 g. Li and Pend have shown that 99% of the braking inputs applied by drivers under normal driving conditions are less than 0.23 g, which is similar to the acceleration values of the first and second driver models [32]. The third driver model pertains to emergency scenarios when the relative distance exceeds $D_{\text{level\_3}}$. This involves urgent braking and steering, suggesting limited space for maneuvering. During these emergency scenarios, the average steering input stands at 0.57 g with a standard deviation of 0.14 g, and the braking input average is 0.69 g with a standard deviation of 0.18 g. By integrating these three distinct driver models, our trajectory prediction framework comprehensively accounts for the inherent uncertainties in driver behaviors, thereby ensuring its responsiveness to varied driving maneuvers produced by the surrounding environmental contexts.

TABLE 1. Mean and standard deviation of driving behavior.

Driver Model		Mean	Standard Deviation	Risk Situation
Normal Brake only	Steering [g]	None	None	Level-1
	Braking rate [g]	0.2	0.05	
Normal both	Steering [g]	0.2	0.05	Level-2
	Braking rate [g]	0.2	0.05	
Emergency	Steering [g]	0.57	0.14	Level-3
	Braking rate [g]	0.69	0.18	

The ability of drivers to undertake avoidance maneuvers serves as an indirect indicator of potential vehicle collisions. Once the driver decides on an evasive action, the direction of steering for both level-2 and level-3 scenarios necessitates further modeling. This work presents a model to capture driver steering preferences. Under the assumption of vehicular movement within a structured road environment, the model employs the approach angle and the offset between the primary and the potentially threatening vehicles to determine steering direction preference.

Fig. 2 illustrates the steering preference direction for the approach angle in forward (rear-end) and oblique collision scenarios, respectively. Specifically, Fig. 2(a) demonstrates that in the context of forward (rear-end) collisions, the probability of steering in either direction remains consistent. However, for oblique collisions, as shown in Fig. 2(b), the steering direction preference is influenced more significantly by the prevailing environmental conditions. This is particularly true in terms of the relative velocity and position deviation between the ego and the dangerous vehicles. For instance, when a threatening vehicle approaches from the right of the ego vehicle, the latter tends to slow down and veer left, distancing itself from the threat. Conversely, if the ego vehicle is positioned to the left of the threatening vehicle, the latter is likely to navigate rightward. This research assigns a probability, contingent upon the approach angle θ, to a specified steering preference direction. The steering preference

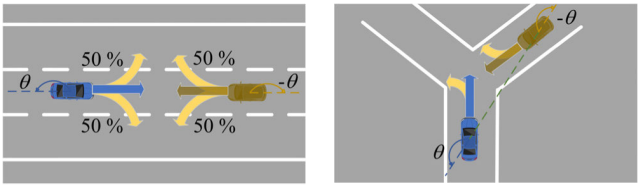

FIGURE 2. Example of the preference for the steering direction. (a) Head-on collision. (b) Oblique collision.

weighting W_θ is shown in (2).

$$W_\theta = 50 \cdot (1 + \sin\theta) \cdot 100\% \tag{2}$$

The equation (2) determined the probability of steering left without considering the offset amounts and guarantees a 50% chance of steering left under head-on or rear-end collisions and a 100% chance of steering left under a pure right-side impact collision.

The preference in steering direction for a vehicle is influenced by both the approach angle between vehicles and the relative displacement deviation between the ego and the threatening vehicles. For a more comprehensive representation of the steering direction preference, an added weight is incorporated to minimize overlap in steering decisions, as depicted in Fig. 3. This designates the pivotal offset amount at which collisions are averted and actions like braking or steering are deemed unnecessary during vehicular motion. The weighting W_{off} for the steering direction can be formulated as in (3).

$$W_{\text{off}} = \begin{cases} \frac{1}{2} \cdot [1 + sign(\cos\theta)], & \Delta l_{\text{off}} \geq l_{\text{offc}} \\ \frac{1}{2} \cdot [1 + sign(\frac{\pi}{2} \cdot \frac{\Delta l_{\text{off}}}{l_{\text{offc}}}) \cdot (sign(\cos\theta))], & |\Delta l_{\text{off}}| > l_{\text{offc}} \\ \frac{1}{2} \cdot [1 - sign(\cos\theta)], & \Delta l_{\text{off}} \leq l_{\text{offc}} \end{cases} \tag{3}$$

where, Δl_{off} represents the lateral relative displacement deviation between the ego and the object vehicle. l_{offc} is the critical offset amount that ensures no collision without any action. $\Delta l_{\text{off}}/l_{\text{offc}}$ reflects the proximity between the object and the ego vehicle. The larger the value of $\Delta l_{\text{off}}/l_{\text{offc}}$, the smaller the danger; conversely, the smaller the value, the greater the danger.

In the context of the prevailing environmental conditions, the probability $P_{\text{steer\_left}}$ of the vehicle making a left turn is articulated as shown in (4). It incorporates the steering preference probability W_θ and a weighting factor W_{off} which accounts for the relative positional deviation in turning.

$$P_{\text{steer\_left}} = W_{\text{off}} \cdot \frac{[1 + cos2\theta] + W_\theta \cdot [1 - \cos 2\theta]}{2} \tag{4}$$

The driver model in this work, which encompasses normal brake only, normal brake and turn, and emergency brake and turn, is determined based on relative distance thresholds ($D_{\text{level\_1}}$, $D_{\text{level\_2}}$, $D_{\text{level\_3}}$). When the driver model indicates steering input (i.e., level-2 and level-3), we employ $P_{\text{steer\_left}}$ to determine the vehicle's future steering direction.

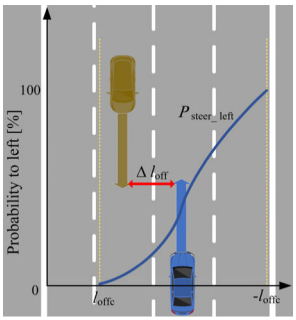

FIGURE 3. Preference for the steering direction depending on the offset.

C. PERCEIVED UNCERTAINTY PROPAGATION BASED ON EKF

Considering the uncertainties associated with sensors and to be in line with practical applications for vehicles and similar systems, it is assumed in this work that all vehicles in the vehicular network are equipped with low-cost onboard GPS receivers and various sensors (e.g., lidar, camera). The propagation of uncertainty can be assessed for any given continuous time. EKF operates by predicting or updating the current state based on the preceding state. Essentially, it leverages control theory to deduce the optimal estimate and covariance matrix for the present moment using the motion model based on the state from the previous time. This iterative process continues for subsequent estimations. By employing the motion system equations and measurement models, along with their associated errors, the Kalman gain is obtained. The filtered values, obtained through this process, are then utilized to rectify errors iteratively, thereby providing an optimal trajectory prediction during vehicle movement.

The system uncertainty is represented by the prior estimate covariance P_t^- at the current time step.

$$P_{t+1}^- = AP_tA^T + Q \tag{5}$$

where, P_t corresponds to the posterior estimate covariance at the previous time step, while Q illustrates the variance of the process noise, serving as a quantifier for the uncertainties inherent in the motion system. This process noise adheres to a standard normal distribution with a mean value of 0 and a standard deviation by Q represented.

The Kalman gain coefficient can be represented as (6):

$$K_{t+1} = \frac{P_{t+1}^- H^T}{HP_{t+1}^- H^T + R} \tag{6}$$

where, K_{t+1} represents Kalman gain coefficient, functioning as a weighting factor to balance the uncertainties between the predicted state and the observed measurements, thereby facilitating the update of the system state. H is referred to

as the observation matrix and is effectively a linearization of the observation model in the vicinity of the current state, commonly realized through the Jacobian matrix. R is the observation noise covariance matrix, which quantifies the uncertainties inherent in the sensing mechanisms. This observation noise follows a standard normal distribution with an expected value of 0 and a standard deviation denoted by R.

As the vehicle moves, the system will accumulate errors, which need to be continuously updated through the covariance matrix.

$$\begin{cases} X_{t+1} = X_{t+1}^{-} + K_{t+1}(Z_{t+1} - HX_{t+1}^{-}) \\ P_{t+1} = (I - HK_{t+1})P_{t+1}^{-} \end{cases} \tag{7}$$

where, X_{t+1} represents the best estimate value at time $t+1$. For the ego vehicle, the relevant parameter is represented by X_v, while for the object vehicle, the corresponding parameter is denoted as X_o. Z_{t+1} is the true value at time $t+1$, P_{t+1} denotes the updated error, and I refers to the identity matrix.

The optimal estimation of the current state is obtained using EKF, serving as the foundation for predicting future motion subject to uncertainties, denoted as X_v and X_o. Subsequent research is grounded on this data.

D. UNCERTAINTY PROPAGATION IN KINEMATIC MOTION MODELS

The possible distribution range of future trajectories for the ego and object vehicle is calculated in the derivation of trajectory uncertainty. This forms the basis for determining whether the state of the ego vehicle is dangerous. Considering that instability and errors can be introduced when linearizing and discretizing a typical nonlinear system, the use of a nonlinear system within the model-based prediction approach is employed in this paper to enhance the robustness of trajectory forecasting. By incorporating the previously discussed driver model into the kinematic model, the predicted trajectory can take into account constraints arising from driver behaviors. Within dynamic environments, the influence of the driver model on the kinematic model is predominantly evident in aspects like lateral and longitudinal velocities, acceleration, and steering angle. As such, these constraint factors are integrated into the Jacobian matrix.

The nonlinear system equation is given as (8):

$$X_{t+1} = f(X_t) + Lw_t \tag{8}$$

where, X_t, X_{t+1} are the system states at time t and $t+1$ respectively. Notably, X_t is derived through EKF to obtain a state at time t. For the ego vehicle, its system state is denoted as X_v, while for the object vehicle, it's denoted as X_o. w_t represent a Gaussian noise which acts as an input to the system state. The matrix L characterizes the mapping of this noise into the state space.

Considering the characteristics, necessary parameters, and suitable operational conditions of the model, the CYRA model for the ego vehicle is opted in this work. The CYRA can be rewritten as (9):

$$\begin{bmatrix} x_v(t+1) \\ y_v(t+1) \\ \phi_v(t+1) \\ v_{xv}(t+1) \\ v_{yv}(t+1) \\ w_v(t+1) \\ a_{xv}(t+1) \\ a_{yv}(t+1) \end{bmatrix} = \begin{bmatrix} v_{xv}(t)cos(\phi_v(t)) - v_{yv}(t)\sin(\phi_v(t)) \\ v_{xv}(t)\sin(\phi_v(t)) + v_{yv}(t)\cos(\phi_v(t)) \\ w_v(t) \\ a_{xv}(t) + v_{yv}(t)w_v(t) \\ a_{yv}(t) + v_{xv}(t)w_v(t) \\ 0 \\ 0 \\ 0 \end{bmatrix} + \begin{bmatrix} 0 & 0 & 0 \\ 0 & 0 & 0 \\ 0 & 0 & 0 \\ 0 & 0 & 0 \\ 0 & 0 & 0 \\ 1 & 0 & 0 \\ 0 & 1 & 0 \\ 0 & 0 & 1 \end{bmatrix} \begin{bmatrix} W_w(t) \\ W_{ax}(t) \\ W_{ay}(t) \end{bmatrix} \tag{9}$$

where, W_{ax} and W_{ay} indicate noise for the longitudinal and lateral acceleration derivatives, and W_w is the noise for the yaw rate derivative.

For object vehicles, considering that their state is measured by the ego vehicle's onboard sensors and can only measure their relative position, angle, and speed to the ego vehicle, a CA model is used for their state prediction.

The expression for CA can be reformulated as shown in (10):

$$\begin{bmatrix} \dot{X}_o(t+1) \\ \dot{Y}_o(t+1) \\ \dot{V}_{xo}(t+1) \\ \dot{V}_{yo}(t+1) \\ \dot{a}_{xo}(t+1) \\ \dot{a}_{yo}(t+1) \end{bmatrix} = \begin{bmatrix} V_{xo}(t) \\ V_{yo}(t) \\ a_{xo}(t) \\ a_{xo}(t) \\ 0 \\ 0 \end{bmatrix} + \begin{bmatrix} 0 & 0 \\ 0 & 0 \\ 0 & 0 \\ 0 & 0 \\ 1 & 0 \\ 0 & 1 \end{bmatrix} \begin{bmatrix} W_{Ax}(t) \\ W_{Ay}(t) \end{bmatrix} \tag{10}$$

where, W_{Ax} and W_{ay} indicate noise for the longitudinal and lateral acceleration derivatives.

The traditional CYRA model does not consider the uncertainty of motion prediction and driver uncertainty, so an improved CYRA model is proposed to describe the impact of uncertainty on trajectory prediction. Firstly, the future trajectory of the vehicle considering driver uncertainty is obtained, and then a normal distribution is used to generate the future trajectory distribution.

The expected value and covariance matrix of the discretized trajectory are derived as (11):

$$\begin{cases} X_{t+1} = F_t X_t \\ \sum_{X_{t+1}} = F_t \sum_{x_t} F_t^T + L_t Q_t L_t^T \end{cases} \tag{11}$$

where, $\sum_{x_t}$ represents the covariance of the system state. For the ego vehicle, its covariance is denoted as $\sum_v$, while for the object vehicle, it's denoted as $\sum_o$. t denotes time. F_t is the Jacobian matrix of the system state at time t. Q_t indicates the covariance matrix of Gaussian noise w_t.

To achieve a cohesive integration of the driver model into the kinematic schema, one must meticulously translate the

salient parameters of the driver model to correspond with those of the kinematic paradigm. Therefore, assuming that the model is a front-wheel-drive model, the steering wheel angle is close to the front-wheel angle.

$$\begin{cases} \beta = \tan^{-1}(\dfrac{l_r}{l_r + l_f} tan(\delta_f)) \\ V_t = \sqrt{v_{xv}^2(t) + v_{yv}^2(t)} \\ \varphi = \displaystyle\int_0^{\Delta t} \frac{V_t \cdot sin(\beta)}{l_r} d\Delta t \end{cases} \tag{12}$$

where, $l_r$and l_f denote the distances from the vehicle center to the front and rear wheels, respectively. βrefers to the slip angle of the ego vehicle, and δ_f indicates the steering angle of the ego vehicle.

For object vehicles, their uncertainty in terms of driver uncertainty and future trajectory distribution is similar to that of the ego vehicle. It should be noted that for object vehicles, the ego vehicle is a dangerous vehicle. For an ego vehicle in level-1, the value of $P_{\text{steer\_left}}$ is set to 50%, and the vehicle follows a linear trajectory. When the vehicle is categorized under level-2 or level-3, a value of $P_{\text{steer\_left}}$ exceeding 50% signifies a leftward turn. In contrast, if the probability $P_{\text{steer\_left}}$ is less than 50%, the vehicle is interpreted as making a rightward turn. Additionally, the mean and covariance of the driver model parameters are integrated into the Jacobian matrix. Based on Table 1, the Jacobian matrix of level 1 that integrates driver uncertainty into the system equation is derived as (13), as shown at the bottom of the next page, the Jacobian matrix of level 2,3 is denoted as in (14), as shown at the bottom of the next page. Based on the aforementioned motion model, we can derive the distribution of the ego vehicle's motion $V = \{X_v^i, \sum_v^i\}_{i=t+1,\ldots,t+N_t}$ and the distribution of the object vehicle's motion $O = \{X_o^i, \sum_o^i\}_{i=t+1,\ldots,t+N_t}$ over N_t future time. Finally, v and o are defined by: $v = (X_v, \sum_v)$ and $o = (X_o, \sum_o)$.

IV. COLLISION RISK ASSESSMENT BASED ON HEURISTIC MONTE CARLO OF TRUNCATED GAUSSIAN DISTRIBUTION

In this section, a deterministic collision detection algorithm based on relative distance is introduced to eliminate unnecessary sampling points, thereby enhancing the algorithm's efficiency and reducing the model's complexity. The deterministic collision detection algorithm is triggered when the vehicle's position falls within areas of absolute safety or absolute danger. A mixed truncated Gaussian filter is employed to exclude points outside the feasible driving area suggested by the kinematic model, thereby modeling the inherent uncertainty in road structures. MC sampling is utilized to calculate collision probabilities, improving MC efficiency by avoiding deterministic risk points and points outside the road boundaries that are definitively unreachable.

A. DETERMINISTIC COLLISION DETECTION

In dynamic driving scenarios, continuous probability collision detection is not requisite at every time step. Such a practice could lead to a significant wastage of computational resources. Moreover, human drivers typically don't overly focus on potential collisions when they perceive vehicles to be within a safe distance range. Given this context, a safety assessment detection algorithm for structured roads in our research is introduced, primarily targeting kinematic model predictions of forward positions at future time steps. The deterministic safety assessment detection determines the likelihood of a collision based on the safe/dangerous zones between the ego and the object vehicle. If both the trajectories of the ego and object vehicle adhere to safety distance standards, a risk assessment can be directly inferred without considering the uncertainty of the trajectories. Otherwise, the uncertainties in the trajectory and the unpredictability of the driver are taken into account to estimate the probability of a collision.

When the combined lateral and longitudinal relative distances between the two vehicles near a predefined dangerous threshold, signifying an impending collision, the collision probability $P_{\text{coll}}^i(v, o)$ at time i is directly assigned a value of 1. When the lateral and longitudinal relative distances between the two vehicles exceed the safety threshold, the situation is deemed safe, and the collision probability is directly assigned a value of 0. If the situation falls between the safety and danger thresholds, the computational method outlined in Section IV-B is described.

The criteria for deterministic safety detection are elucidated in (15), as shown at the bottom of the next page.

where, L_v, d_v, L_o, d_o represent the length and width of the ego and object vehicle;$v_v = \sqrt{v_{xv}^2 + v_{yv}^2}$ is the traveling speed of the ego vehicle; ΔL denotes a parameter related to the vehicle's body length; Δd refers to lateral safety distances; α, β are respectively angles between the diagonal line from the center point of the ego vehicle to its corners and its short side and long side; $\Delta\phi||$ is the absolute value of the difference in yaw angle between both vehicles.

B. ROAD UNCERTAINTY BASED ON TRUNCATED GAUSSIAN DISTRIBUTION

In the probabilistic model for MDU-CRA, it's vital to account for the effects of unreachable areas shaped by road boundaries and other factors. As illustrated in Fig. 4, vehicles are improbable to venture outside these boundaries, thereby preventing unrealistic accidents or collisions.

Guided by heuristic insights, the vehicle's trajectory is sampled via a truncated Gaussian distribution. This ensures dense sampling within feasible regions while sparsely sampling in inaccessible zones. By eliminating outliers or extreme values, the modeling of the vehicle collision risk is further refined, significantly enhancing the precision of estimations and forecasts.

Considering the inherent intricacy of multidimensional distributions that precludes straightforward expression derivations, we focus on a multi-dimensional variable set $X_v = [x_v, y_v, \phi_v]^T, X_o = [x_o, y_o]^T$. Using the ego vehicle v as a

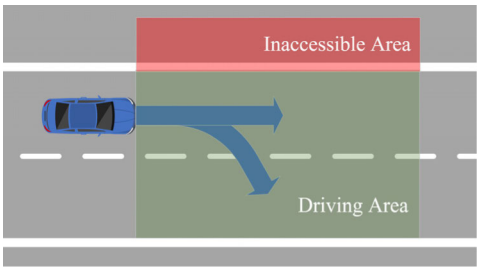

FIGURE 4. Inaccessible area diagram.

representative example (the computational approach remains analogous for both the ego and object vehicle), the truncated Gaussian probability density function (pdf) $p_v(X)$ having corresponding covariance matrix $\sum_v$ and mean X_v is delineated in (16).

$$p_v(X) = \frac{1}{2\pi^{3/2}|\sum_v|^{1/2}} \cdot \frac{\exp(-\frac{1}{2}(X - X_v)^T \sum_v^{-1}(X - X_v))}{\int_{a_x}^{b_x}\int_{a_y}^{b_y}\int_{a_\phi}^{b_\phi} p_v(X)\, d\theta dy dx} \tag{16}$$

where, $X = [x, y, \phi]^T$ is a random variable vector. The determinant of the covariance matrix $\sum_v$ is denoted as $|\sum_v|$, while the covariance matrix $\sum_v$ is obtained from the controlled ego vehicle. We adopt an integral formulation to normalize the pdf $p_v(X)$ within a specified truncation interval. This normalization ensures that the function represents a valid probability distribution over the state space of interest, thereby facilitating accurate statistical inference.

Considering the uncertainties in state estimation and driver behavior, short-term motion prediction trajectories that align with human cognition can be derived. The pdf of an ego vehicle v and an object vehicle o are denoted $p_v(X)$ and $p_o(X)$.

C. COLLISION RISK ASSESSMENT BASED ON HEURISTIC MONTE CARLO

The external shape of vehicles is approximated as rectangles to model them. This results in an uncertainty region representing potential positions or states of a vehicle. Subsequently, the possibility of spatial conflicts or potential collisions is

$$F_{t+1} = \begin{bmatrix} 0 & 0 & \begin{matrix}-(v_{xv}(t) + a_{xv}(t)\cdot\Delta t)\sin(\phi(t)) \\ -v_{yv}(t)\cos(\phi(t))\end{matrix} & \cos(\phi(t)) & -\sin(\phi(t)) & 0 & 0 & 0 \\ 0 & 0 & \begin{matrix}(v_{xv}(t) + a_{xv}(t)\cdot\Delta t)\cos(\phi(t)) \\ -v_{yv}(t)\sin(\phi(t))\end{matrix} & \sin(\phi(t)) & \cos(\phi(t)) & 0 & 0 & 0 \\ 0 & 0 & 0 & 0 & 0 & 1 & 0 & 0 \\ 0 & 0 & 0 & 0 & \omega(t) & v_{yv}(t) & 1 & 0 \\ 0 & 0 & 0 & -\omega(t) & 0 & -(v_{xv}(t) + a_{xv}(t)\cdot\Delta t) & 0 & 1 \\ 0 & 0 & 0 & 0 & 0 & 0 & 0 & 0 \\ 0 & 0 & 0 & 0 & 0 & 0 & 0 & 0 \\ 0 & 0 & 0 & 0 & 0 & 0 & 0 & 0 \end{bmatrix} \tag{13}$$

$$F_{t+1} = \begin{bmatrix} 0 & 0 & \begin{matrix}-(v_{xv}(t) + a_{xv}(t)\cdot\Delta t)\sin(\phi(t)) \\ -(v_{yv}(t) + a_{yv}(t)\cdot\Delta t)(t)\cos(\phi(t))\end{matrix} & \cos(\phi(t)) & -\sin(\phi(t)) & 0 & 0 & 0 \\ 0 & 0 & \begin{matrix}(v_{xv}(t) + a_{xv}(t)\cdot\Delta t)\cos(\phi(t)) \\ -(v_{yv}(t) + a_{yv}(t)\cdot\Delta t)(t)\sin(\phi(t))\end{matrix} & \sin(\phi(t)) & \cos(\phi(t)) & 0 & 0 & 0 \\ 0 & 0 & 0 & 0 & 0 & 1 & 0 & 0 \\ 0 & 0 & 0 & 0 & \omega(t) & (v_{yv}(t) + a_{yv}(t)\cdot\Delta t)(t) & 1 & 0 \\ 0 & 0 & 0 & -\omega(t) & 0 & -(v_{xv}(t) + a_{xv}(t)\cdot\Delta t) & 0 & 1 \\ 0 & 0 & 0 & 0 & 0 & 0 & 0 & 0 \\ 0 & 0 & 0 & 0 & 0 & 0 & 0 & 0 \\ 0 & 0 & 0 & 0 & 0 & 0 & 0 & 0 \end{bmatrix} \tag{14}$$

$$\begin{cases} P^i_{\text{coll}} = 0, \begin{cases} \left|(x^i_v - x^i_o)\cos(\phi^i_v) + (y^i_v - y^i_o)\sin(\phi^i_v)\right| \geq 0.5(\sqrt{L_v^2 + d_v^2}\sin(\alpha + |\Delta\varphi|) + L_o) + 1.2v_v \\ or \\ \left|(y^i_v - y^i_o)\cos(\phi^i_v) + (x^i_v - x^i_o)\sin(\phi^i_v)\right| \geq 0.5(\sqrt{L_v^2 + d_v^2}\sin(\beta + |\Delta\varphi|) + d_o) + \Delta d \end{cases} \\ P^i_{\text{coll}} = 1, \begin{cases} \left|(x^i_v - x^i_o)\cos(\phi^i_v) + (y^i_v - y^i_o)\sin(\phi^i_v)\right| \leq 0.5(\sqrt{L_v^2 + d_v^2}\sin(\alpha + |\Delta\varphi|) + L_o) + \Delta L \\ or \\ \left|(y^i_v - y^i_o)\cos(\phi^i_v) + (x^i_v - x^i_o)\sin(\phi^i_v)\right| \leq 0.5(\sqrt{L_v^2 + d_v^2}\sin(\beta + |\Delta\varphi|) + d_o) + \Delta d \end{cases} \end{cases} \tag{15}$$

Algorithm 1 Collision Risk Assessment Considering the Multi-Dimensional Uncertainties (MDU-CRA) Algorithm

Input: Data matrix X_v, X_0. X_v, X_0 are the state parameters of the ego and the object vehicle respectively.

Output: Collision probability $P_{\text{coll}}(v, o)$. //Output future collision risk in 2 seconds

1. $[x_v, y_v, \phi_v, v_{xv}, v_{yv}, \omega_v, a_{xv}, a_{yv}]$ $=EKF(X_v)$;//Update ego status via EKF;
2. $[x_o, y_o, v_{xo}, v_{yo}, a_{xo}, a_{yo}]$ $=EKF(X_0)$;//Update object status via EKF;
3. $[drive_1, drive_2, drive_3]$=$buildDriverModel()$;
4. $\{X_v^i, \sum_v^i\}_{i=1,\ldots,N_t}$ =CYRA(X_v, $drive_1$, $drive_2$, $drive_3$);// Ego vehicle $X_v^i = [(x_v^{i,1}, y_v^{i,1}, \phi_v^{i,1}), \ldots, (x_v^{i,N_t}, y_v^{i,N_t}, \phi_v^{i,N_t})]$
5. $\{X_o^i, \sum_o^i\}_{i=1,\ldots,N_t}$ =CA(X_0, $drive_1$, $drive_2$, $drive_3$);//object vehicle $X_o^i = [(x_o^{i,1}, y_o^{i,1}), \ldots, (x_o^{i,N_t}, y_o^{i,N_t})]$
6. **for** $i \leftarrow 1$ to N_t **do** //N_t is number of the future trajectories
7. **if** $\left|(x_v^i - x_o^i)cos(\phi_v) + (y_v^i - y_o^i)sin(\phi_v^i)\right|$ or $\left|(y_v^i - y_o^i)cos(\phi_v) + (x_v^i - x_o^i)sin(\phi_v^i)\right| \geq D_{\text{safety}}$ **then**
8. $P_{\text{coll}}(v, o) = 0$;
9. **break**;
10. **else if** $\left|(x_v^i - x_o^i)cos(\phi_v^i) + (y_v^i - y_o^i)sin(\phi_v)\right|$ or $\left|(y_v^i - y_o^i)cos(\phi_v) + (x_v^i - x_o^i)sin(\phi_v^i)\right| \leq D_{\text{danger}}$ **then**
11. $P_{\text{coll}}(v, o) = 1$;
12. **break**;
13. **else**
14. **for** $j \leftarrow 1$ to N_c **do** //N_c is the total number of MC samples
15. $(x_v^{i,j}, y_v^{i,j}, \phi_v^{i,j})$ $=randc(\phi p_v((x_v^{i,j}, y_v^{i,j}, \phi_v^{i,j}))$;
16. $(x_o^{i,j}, y_o^{i,j})$ $=randc(p_o((x_o^{i,j}, y_o^{i,j}))$;
17. **if** $S_v(x_v^{i,j}, y_v^{i,j}, \phi_v^{i,j}) \cap S_o(x_o^{i,j}, y_o^{i,j}) \neq \emptyset$ **then**
18. $P_{\text{coll}}^{i,j}(v, o)$ =1;
19. **else**
20. $P_{\text{coll}}^{i,j}(v, o)$ =0;
21. **end if**
22. **end for**
23. $P_{\text{coll}}^i(v, o) = \frac{\sum_{j=1}^{N_c} 2P_{\text{coll}}^{i,j}(v,o)}{N_c}$;
24. **end if**
25. **end for**
26. $P_{\text{coll}}(v, o)$ $=max([P_{\text{coll}}^1(v, o), \ldots, P_{\text{coll}}^{N_t}(v, o)])$;
27. **return** $P_{\text{coll}}(v, o)$;

determined by checking if the uncertainty regions of two vehicles overlap. Leveraging the expected value and the covariance matrix of the joint pdf, the system can compute the vehicle's collision probability.

As shown in Fig. 5, $S_v \cap S_o \neq \emptyset$ indicates that there is an intersection between the spatial positions occupied by the ego and object vehicle, i.e., a collision occurs between them. S_v, S_o represent the spatial positions occupied by the ego and object vehicle at the current time, respectively. They are the safety zone boundaries represented by the outer envelope expansion of the geometric shapes of the ego and object vehicle.

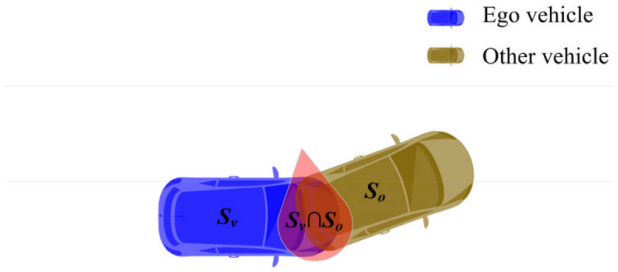

FIGURE 5. Diagram of collision between ego and object vehicle.

The Multi-Dimensional Uncertainties-CRA determines the likelihood of a collision between the ego vehicle and a specific object at a given instant. To assess the risk, the collision probability between the ego and the object vehicle must be repeatedly computed at various predicted times. To address the complexity of the integral computation, the Monte Carlo simulation method is employed to solve the aforementioned equation. The MC method operates on a foundational principle: it commences by randomly sampling variables pertinent to the problem, adhering to their genuine mathematical distributions, across a voluminous dataset. For each of these sampled values, simulated experiments are conducted to ascertain the occurrence of an event. Subsequently, its probability is estimated based on the event's recurrence rate. The uncertainty surrounding a vehicle's state aligns with the Gaussian joint probability distribution. Considering the differences in shapes between the ego and the object vehicle, the Monte Carlo method is used to calculate the collision probability $P_{\text{coll}}^i(v, o)$ represented by (17):

$$\begin{cases} I_{\text{coll}}^i(S_v(p_v(x_v^{i,j}, y_v^{i,j}, \phi_v^{i,j})), S_o(p_o(x_o^{i,j}, y_o^{i,j}))) \\ \quad = \begin{cases} 0, S_v(x_v^i, y_v^i, \phi_v^i) \cap S_o(x_o^i, y_o^i) = \emptyset \\ 1, S_v(x_v^i, y_v^i, \phi_v^i) \cap S_o(x_o^i, y_o^i) \neq \emptyset \end{cases} \\ P_{\text{coll}}^i(v, o) = \dfrac{1}{N_c} \displaystyle\sum_{j=1}^{N_c} I_{\text{coll}}^i(S_v(p_v(x_v^{i,j}, y_v^{i,j}, \phi_v^{i,j})), \\ \qquad S_o(p_o(x_o^{i,j}, y_o^{i,j}))) \end{cases} \tag{17}$$

where, N_c represents the total number of MC samples for the position of the ego vehicle and object vehicle. j is the j-th sampling. $((x_v^{i,1}, y_v^{i,1}, \phi_v^{i,1}),\ldots,(x_v^{i,N_c}, y_v^{i,N_c}, \phi_v^{i,N_c}))$ and $((x_o^{i,1}, y_o^{i,1}),\ldots,(x_o^{i,N_c}, y_o^{i,N_c}))$ are samples generated by following the distribution of the ego vehicle $p_v(X)$ and the distribution of the obj vehicle $p_o(X)$ at time i. $I_{\text{coll}}^i(S_v(p_v(x_v^{i,j}, y_v^{i,j}, \phi_v^{i,j})), S_o(p_o(x_o^{i,j}, y_o^{i,j})))$ is a collision test between the S_v of the ego vehicle and the $S_o$of the object vehicle at time i.

The MDU-CRA algorithm is as shown in algorithm 1. Between lines 1 and 2, the EKF is employed to derive realistic motion states for both the ego vehicle and the object vehicle. The development of a driver model is indicated in the 3 line, where $drive_1$, $drive_2$ and $drive_3$ respectively represent normal brake only, normal brake and turn, and emergency brake and turn. Kinematic models are leveraged in lines 4 and 5 to

TABLE 2. Parameters of all experiments.

Symbol	Description	Unit	Value
·	Normal Brake only/Braking rate /Mean and Standard Deviation	g	0.2/0.05
·	Normal both/Steering/Mean and Standard Deviation	g	0.2/0.05
·	Normal both/Braking rate/Mean and Standard Deviation	g	0.2/0.05
·	Emergency/Steering/Mean and Standard Deviation	g	0.57/0.14
·	Emergency/Braking rate/Mean and Standard Deviation	g	0.69/0.18
l_{offc}	The critical offset of the vehicle without collision , braking, steering	m	1.89
l_r, l_f	The distances from the vehicle center to the front/rear wheel	m	1.85
L_h, L_o	The length of the ego/object vehicle	m	5.25
d_v, d_o	The width of the ego/object vehicle	m	1.85
a_x,b_x	The upper/lower truncation values of the X-axis	·	·
a_y,b_y	The upper/lower truncation values of the Y-axis when in the outermost lane	m	±1.75
a_ϕ , b_ϕ	The upper/lower truncation values of the steering angle when in the outermost lane	·	·
N_t, N_c	The number of predicted future trajectories/MC sampling	·	5/1000
EKF			
Q	Measurement noise Q of the ego's sensor	·	diag(100*ones(1,8))
R	Measurement noise R of the ego's sensor	·	diag([0.32,0.32,0.04,0.1,0.05,0.1,0.1,0.05])
H	Measurement noise H of the ego's sensor	·	diag(ones(1,8))
L	Hyperparameters of the ego vehicle	·	[0,0,0;0,0,0;0,0,0;0,0,0;0,0,0;0,0,0;1,0,0;0,1,0;0,0,1]

TABLE 3. RMSE and ADE values of prediction error.

Evaluation Metric	Prediction horizon (s)	PMETP	MDU-CRA
RMSE (m)	1	0.81	0.42
	2	1.56	1.47
ADE	1	0.74	0.33
	2	1.45	1.09

forecast forthcoming trajectories for both vehicles. In lines 7 to 13, deterministic collision detection is adopted, primarily relying on the relative distance metric to distinguish between benign and perilous situations. Here, D_{safety} embodies the superior portion of Equation (16)'s right-hand side; its value domain is largely influenced by the current vehicle speed. Conversely, D_{danger} symbolizes the inferior segment of Equation (16)'s right-hand side, with its amplitude chiefly swayed by vehicular geometry. In conclusion, the truncated Gaussian distribution is incorporated in tandem with MC sampling in lines 15 to 25 to quantify collision probabilities. In line 26, the conclusive collision risk is determined by selecting the median of the maximal probabilities foreseen.

V. PERFORMANCE EVALUATION

In order to evaluate the proposed collision risk assessment method considering the multi-dimensional uncertainties, two experiments are performed in this section. Two driving scenarios are extracted and reconstructed from the NGSIM dataset for validation and evaluation, i.e., an active lane-change scenario and an emergency braking scenario. The proposed MDU-CRA algorithm is compared to the probabilistic multi-modal expected trajectory prediction (PMETP)

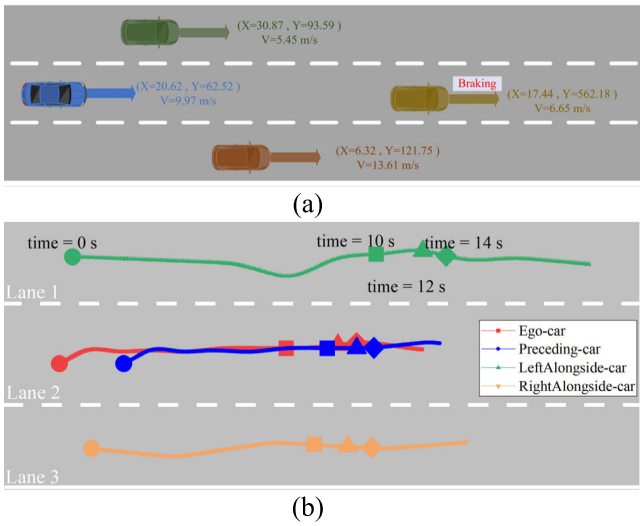

FIGURE 6. Emergency braking scenario (a) Scenario I: schematic diagram of the location for the emergency braking scenario. (b) trajectories of ego vehicle and objects in scenario I.

[33] trajectory predictor in terms of short-term motion prediction accuracy. The efficacy of our risk assessment model is gauged by benchmarking against a range of state-of-the-art models [26], [34] and employing multiple evaluation metrics.

A. EXPERIMENTAL SETTINGS

1) EVALUATION ENVIRONMENT SETTING

Active lane-change scenarios and emergency braking scenarios were extracted from the NGSIM dataset [35]. The sampling points were set at 1000, with a calculation speed of approximately 0.001 seconds, facilitating real-time

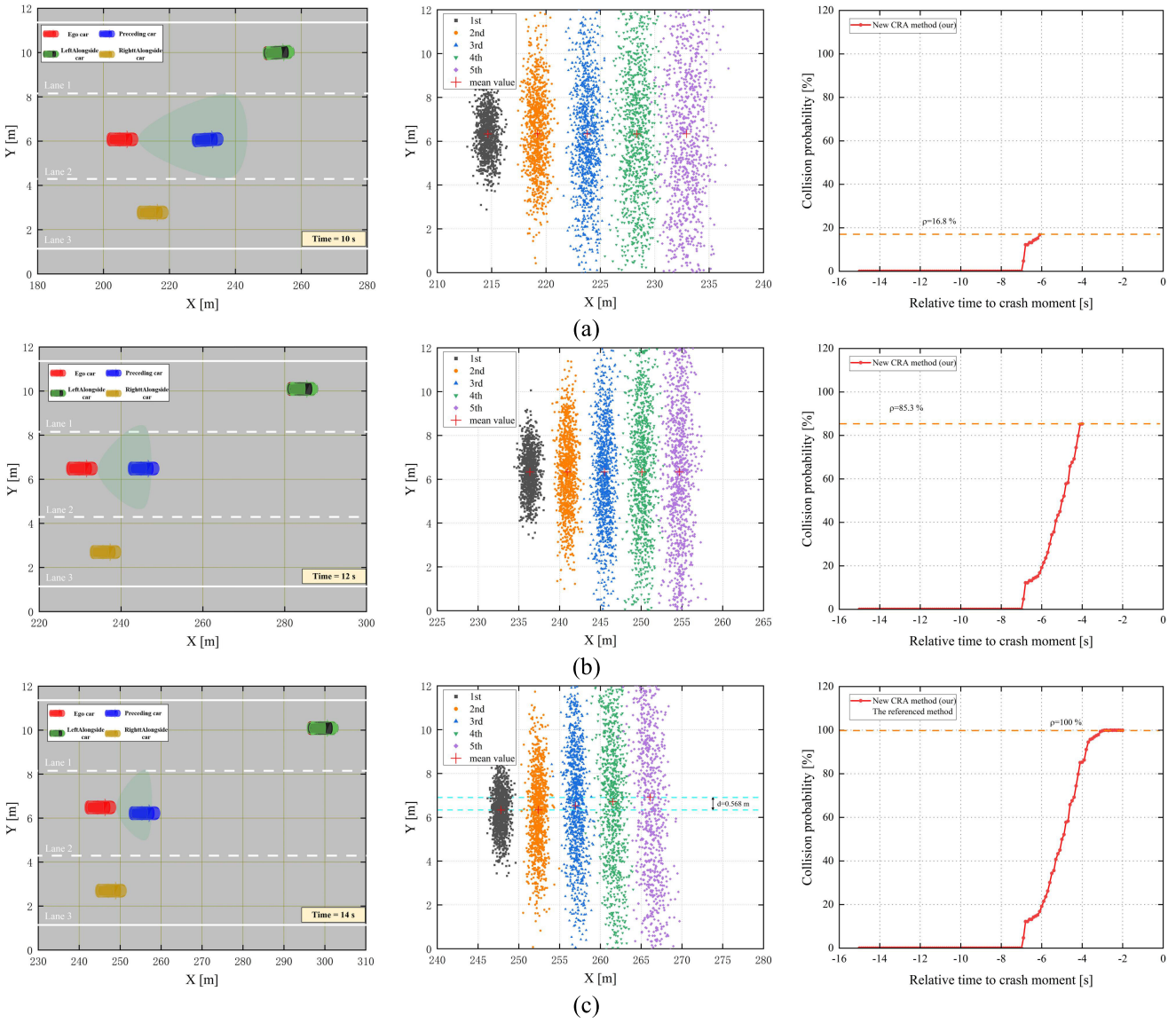

FIGURE 7. Results of emergency braking scenario (a) t=10 s (b) t=12 s (c) t=14 s.

operation. The relevant experiments for this work were conducted using MATLAB 2021, and data pre-processing was completed using Python 3.8. The parameters of all experiments are presented in Table 2.

B. EXPERIMENTAL RESULTS

1) PRECISION COMPARISON OF TRAJECTORY PREDICTION

In this work, a comparative assessment is conducted between our newly introduced trajectory prediction model, which incorporates multi-dimensional uncertainties, and the PMETP approach over a 2-second prediction span. The effectiveness of both models is evaluated using Root Mean Square Error (RMSE) and Average Displacement Error (ADE) as the primary metrics. The Sequence to Sequence (seq2seq) encoder-decoder framework is employed by the PMETP model, amalgamating features of the predicted vehicle and its neighboring vehicles into an LSTM to holistically represent the vehicular context. Additionally, PMETP demonstrates proficient end-to-end training capabilities for on-site traffic scenarios.

From Table 3, it can be observed that our proposed trajectory prediction model, which takes into account multidimensional uncertainty, has smaller RMSE and ADE in short-term prediction compared to the LSTM-based model. Therefore, our trajectory prediction model exhibits a higher level of predictive accuracy.

2) THE EFFICACY OF RISK ASSESSMENT

In this work, a detailed comparative analysis is conducted on risk assessment, employing ordinary evaluation metrics like Advanced Collision Detection Time (ACDT), Time-to-Collision (TTC), and Time Headway (THW), with a focus on scenarios such as emergency braking and active lane changes.

The methods proposed in this article and in [26] and [34] were implemented and evaluated using python. Reference [34] involves an integration of Autoware with a Cooperative Collision Warning System (CCWS) to predict future trajectories and assess collision risks. Reference [26] initially constructs the geometric shapes of lanes using OpenStreetMap (OSM) to determine an initial coarse risk classification, followed by a more comprehensive estimation of criticality.

ACDT stands as a paramount metric in the context of inter-vehicle collision detection. By providing timely and accurate predictions of potential collisions, ACDT empowers drivers with the foresight to initiate preemptive maneuvers. An extended window for driver response is provided by the heightened ACDT, highlighting the robustness of the MDU-CRA in accommodating potential system latency and egress timings.

$$ACDT = t_c - t_d \tag{18}$$

where t_c and t_d, respectively, denote the time a crash occurs and is detected.

TTC [36] and THW [37] serve as pivotal tools for accident prevention and the assessment of driving behavior, commonly employed within the safety algorithms of autonomous driving systems to determine the critical junctures for evasive actions. In accordance with German traffic regulations and the study presented in [35], the typical value for TTC is set at 2.6 s, while THW is determined to be 0.9 s. The formulas for TTC and THW are depicted in equation (19).

$$\begin{cases} TTC = \dfrac{x_o - x_v}{v_{xv} - v_{xo}} \\ THW = \dfrac{x_o - x_v}{v_{xv}} \end{cases} \tag{19}$$

- Scenario I: Emergency braking

Scenario I focuses on the sudden deceleration of a preceding vehicle and its associated collision probability evaluation. Fig. 6(a) depicts the ego vehicle trailing the preceding vehicle on a dual-lane road. After covering a designated distance, the preceding vehicle decelerates abruptly, coming to a halt. Within this deceleration scenario, Fig. 6(b) illustrates the trajectories of the ego vehicle and the neighboring traffic. The ego and preceding vehicles' trajectories are marked in red and blue, respectively. Concurrently, the left and right object vehicles follow paths depicted in green and orange, respectively. It is pertinent to highlight that modifications were made to the NGSIM dataset for this experimental evaluation. Specifically, in the event of a preceding vehicle's deceleration, the ego vehicle initially reduces its speed, thereafter sustaining a consistent velocity for continued progression. This adaptation was incorporated to thoroughly assess the efficacy of the proposed MDU-CRA approach.

Fig. 7 presents schematic representations of the vehicle's state at 10 s, 12 s, and 14 s. It also illustrates the probability distribution maps for predicted trajectories and the associated collision likelihoods. On the left side of Fig. 7(a) to 7(c), the dynamic changes in the feasible driving area for the ego vehicle at distinct time instances are evident. Specifically, as the ego vehicle approaches the threatening vehicle, its maneuvering space becomes increasingly constricted. Conversely, the probability distribution of the ego vehicle's projected trajectories over the next 2 seconds, sampled at 0.4-second intervals, is displayed on the right side of Fig. 7(a) to 8(c). The consequent collision probabilities for these instances are 16.8%, 85.3%, and 100% respectively. A critical observation at t=14 s is that the average trajectory for the fifth step shifts by 0.568 m to the left in contrast to the primarily horizontal orientations of the first and second steps. This deviation signifies a common driver behavior: as one nears a potential threat on the road, there's an instinctual swerve away from the perceived danger to avert possible collisions.

Fig. 8 illustrates the performance comparison of our proposed method with those baselines in [26] and [34] under the scenario of the lead vehicle executing an emergency braking maneuver, as well as the analysis employing various

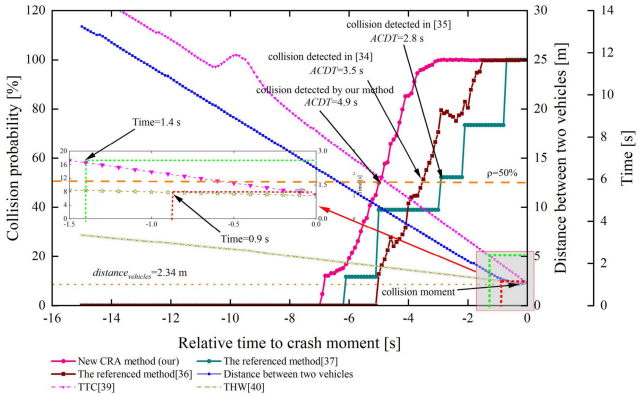

FIGURE 8. Collision probability estimates' evaluation.

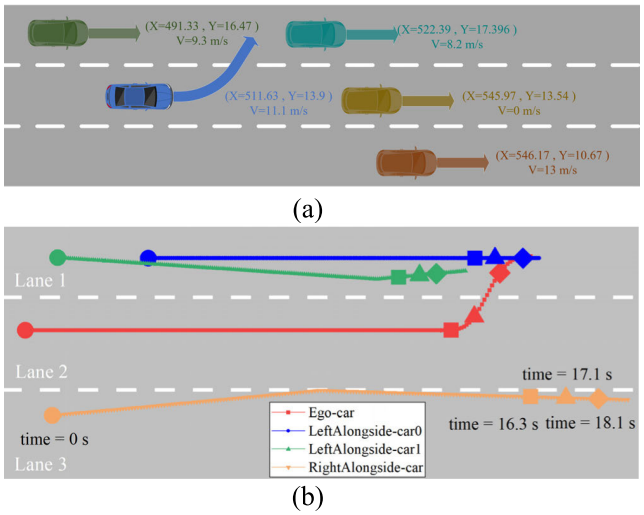

FIGURE 9. An lane-changing driving scenario (a) Scenario II:schematic diagram of the location for the Lane-changing driving scenario.(b) trajectories of ego vehicle and objects in scenario II.

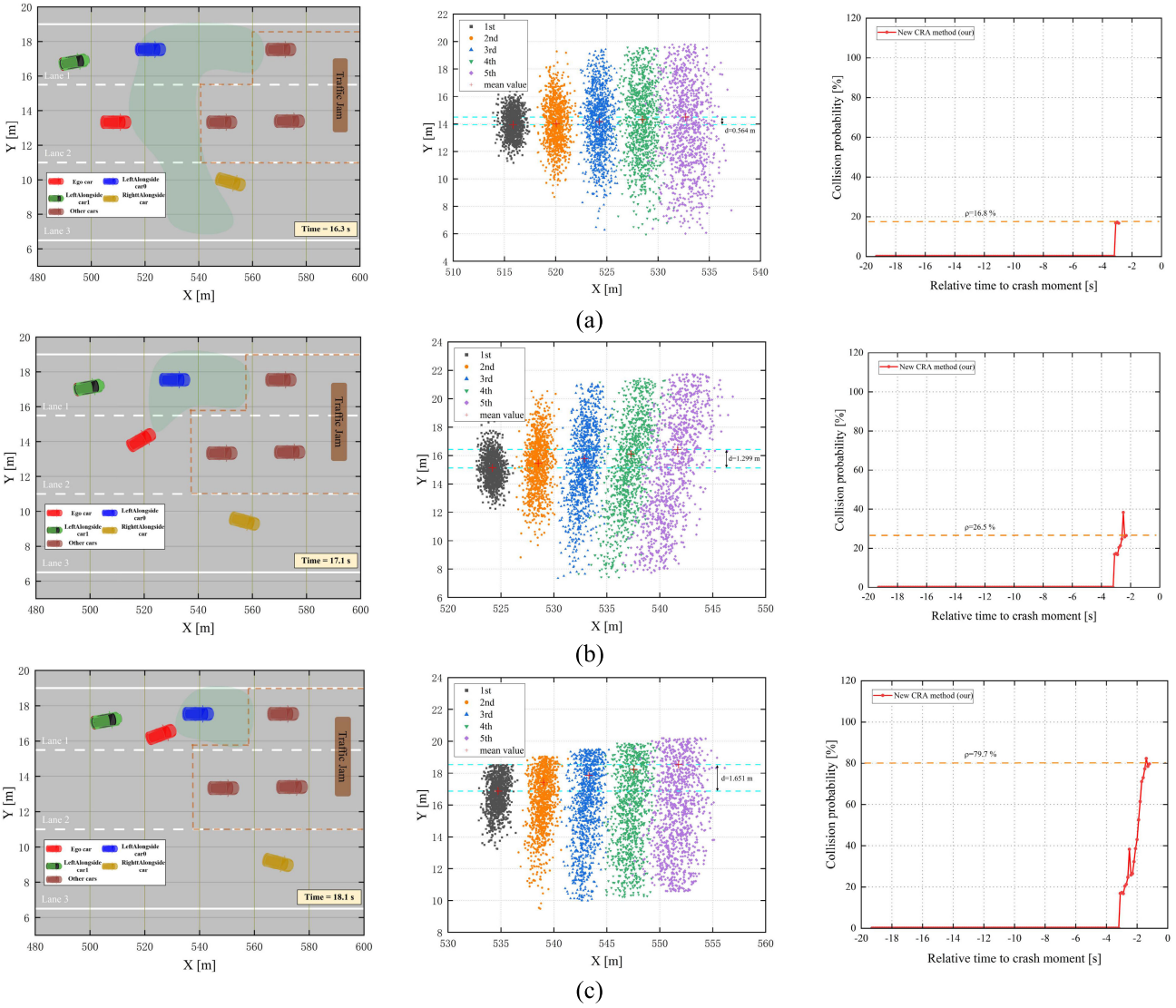

FIGURE 10. Results of lane-changing scenario (a) t=16.3 s (b) t=17.1 s (c) t=18.1 s.

evaluation metrics. As the temporal progression ensues and the inter-vehicular distance diminishes, there's a concomitant escalation in the collision probability. Intriguingly, the collision probability trajectory of our model manifests a steeper ascent than the referenced method.

Assuming an alarm is triggered by the system when the collision probability exceeds 50%, an ACDT value of 4.9 seconds is exhibited by our method, surpassing the ACDT values reported in [26] and [34], which are 2.8 seconds and 3.5 seconds, respectively. In terms of the preset TTC and THW thresholds, the alarm signals are activated at approximately 1.4 seconds and 0.9 seconds, respectively. This demonstrates that a substantially earlier warning time in the longitudinal evaluation process is provided by our model, indicating its superiority. The notable efficacy of our approach is primarily attributable to its state-centric sampling which, compared to static interval-based methods, delivers a more pragmatic representation.

- Scenario II: Lane-changing

Scenario II delineates a situation where the ego vehicle is engaged in a lane transition. In Fig. 9(a), the transition of the vehicle from lane 2 to the less-congested lane 1 after traversing a certain distance is illustrated. In Fig. 9(b), the trajectories of the ego vehicle are elaborated upon in relation to the surrounding traffic during this lane change. Here, the ego vehicle and the potentially perilous vehicles are represented by the red and blue trajectories, respectively, while other surrounding objects are signified by the green and orange trajectories.

A visual representation of the evolving scenario at intervals of 16.3 s, 17.1 s, and 18.1 s is provided by Fig. 10, concurrently showcasing the probabilistic distributions associated with the predicted trajectories and their respective collision likelihoods. As depicted on the left side of Fig. 10(a)∼(c), the permissible driving envelope for the ego vehicle gradually contracts with the passage of time. Given the absence of

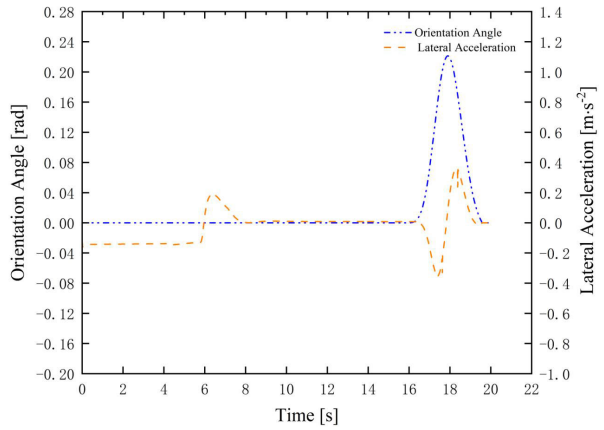

FIGURE 11. Lateral acceleration and orientation angle of ego vehicle in Lane-changing scenario.

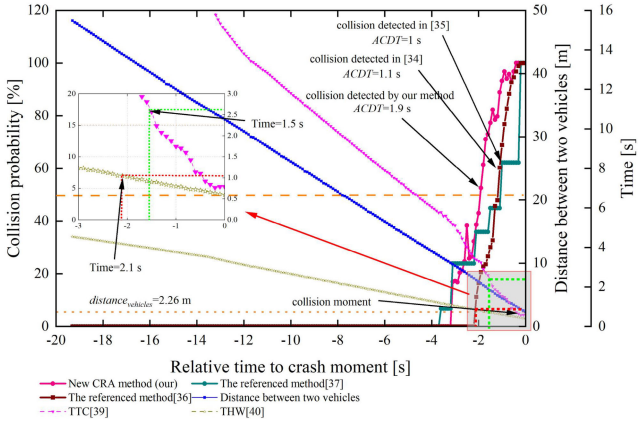

FIGURE 12. Collision probability estimates' evaluation.

an outermost lane during the lane maneuver, a truncated Gaussian function is judiciously employed to sample within the lane, guided by the lane parameters, and to exclude regions beyond the lane boundary. This deliberate approach augments the collision prediction accuracy. The ensuing plots in Fig. 10(a)∼(c) articulate the probabilistic trajectory distributions of the ego vehicle for a predicted horizon of 2 s, sampled at intervals of 0.4 s, and reveal collision probabilities of 16.8%, 26.5%, and 79.7%, respectively. Taking into account typical driver behaviors, the averaged trajectory projections for the ego vehicle over the 2 s window progressively align with the target lane, registering maximum deviations of 0.564 m, 1.299 m, and 1.651 m, in sequence. This modeling aligns coherently with real-world vehicle movement patterns.

In Fig. 11, the variation and boundary constraints associated with the steering angle and lateral acceleration of the ego vehicle throughout the active lane transition in Scene II are illustrated. Upon completion of the maneuver, both metrics – the steering angle and lateral acceleration – revert to a null state.

In Fig. 12, the processes involving our model, various state-of-the-art models, and different evaluation metrics within the context of active lane-changing scenarios are delineated. In terms of ACDT, a value of 1.9 seconds is recorded by our model when the collision probability exceeds 50%, while ACDT values of 1.1 seconds and 1 second are reported in [26] and [34], respectively. For TTC and THW, the times at which the alarm signals are activated are 2.1 seconds and 1.5 seconds, correspondingly. It is evident that, compared to other reference models, an approximately 1-second time advantage in ACDT is offered by our model, capable of issuing warnings 2 seconds prior to a potential collision. However, during the active lane-changing process, the performance of our model is close to that of THW but surpasses that of the TTC metric.

Based on the parameter evaluations in the aforementioned scenarios, superiority over other advanced metrics is demonstrated by our proposed model, making it suitable for the situational assessment modules of assisted driving or autonomous driving systems.

VI. CONCLUSION

This paper presents an MDU-CRA framework designed to account for multidimensional uncertainties, including driver behavior, sensor perception, motion prediction models, and road structure. This algorithm enables the estimation of future risks related to surrounding vehicles, allowing autonomous vehicles to safely handle dangerous driving situations and proactively avoid or mitigate potential collisions. Firstly, we propose a deterministic collision detection algorithm based on relative distance, which enhances efficiency by eliminating unnecessary sampling points. Secondly, our trajectory prediction model combines three different driver intentions with vehicular kinematic models, incorporating a Gaussian truncation function along with Monte Carlo sampling techniques for the prediction of future driving risks. This comprehensive approach ensures autonomous vehicles account for uncertainties in driver behavior, motion prediction models, and road structure when navigating conditions that involve turns and deceleration. Validation is conducted through sudden braking and lane-changing scenarios from the NGSIM dataset. Experimental outcomes underscore our model's capability to preemptively discern impending collisions with a lead time of 1-2 s compared to conventional models, with the projected trajectory probability distribution closely mirroring real-world vehicular movements.

Nevertheless, this research has potential for further refinement. Currently, our focus is primarily on vehicular dynamics models, which might compromise long-range accuracy. Our forthcoming efforts involve the incorporation of neural network methodologies into risk assessment, with a specific focus on the integration of attention-driven mechanisms and graph neural networks to discern inter-vehicular social interactions. This aims to enhance the overall intelligence of vehicular collectives.

REFERENCES

[1] C. Huang, P. Hang, Z. Hu, and C. Lv, "Collision-probability-aware human–machine cooperative planning for safe automated driving," *IEEE Trans. Veh. Technol.*, vol. 70, no. 10, pp. 9752–9763, Oct. 2021.

[2] C. Katrakazas, M. Quddus, and W.-H. Chen, "A new integrated collision risk assessment methodology for autonomous vehicles," *Accident Anal. Prevention*, vol. 127, pp. 61–79, Jun. 2019.

[3] H.-S. Tan and J. Huang, "DGPS-based vehicle-to-vehicle cooperative collision warning: Engineering feasibility viewpoints," *IEEE Trans. Intell. Transp. Syst.*, vol. 7, no. 4, pp. 415–428, Dec. 2006.

[4] J. Hillenbrand, A. M. Spieker, and K. Kroschel, "A multilevel collision mitigation approach—Its situation assessment, decision making, and performance tradeoffs," *IEEE Trans. Intell. Transp. Syst.*, vol. 7, no. 4, pp. 528–540, Dec. 2006.

[5] S. Noh and K. An, "Decision-making framework for automated driving in highway environments," *IEEE Trans. Intell. Transp. Syst.*, vol. 19, no. 1, pp. 58–71, Jan. 2018. [Online]. Available: http://ieeexplore.ieee.org/document/7907201/

[6] K. Chu, M. Lee, and M. Sunwoo, "Local path planning for off-road autonomous driving with avoidance of static obstacles," *IEEE Trans. Intell. Transp. Syst.*, vol. 13, no. 4, pp. 1599–1616, Dec. 2012.

[7] N. Kaempchen, B. Schiele, and K. Dietmayer, "Situation assessment of an autonomous emergency brake for arbitrary vehicle-to-vehicle collision scenarios," *IEEE Trans. Intell. Transp. Syst.*, vol. 10, no. 4, pp. 678–687, Dec. 2009.

[8] D. Ferguson, M. Darms, C. Urmson, and S. Kolski, "Detection, prediction, and avoidance of dynamic obstacles in urban environments," in *Proc. IEEE Intell. Vehicles Symp.*, Jun. 2008, pp. 1149–1154.

[9] Z. Yang, C. Shi, Y. Zheng, and S. Gu, "A study on a vehicle semi-active suspension control system based on road elevation identification," *PLoS ONE*, vol. 17, no. 6, Jun. 2022, Art. no. e0269406.

[10] D. Greene, J. Liu, J. Reich, Y. Hirokawa, A. Shinagawa, H. Ito, and T. Mikami, "An efficient computational architecture for a collision early-warning system for vehicles, pedestrians, and bicyclists," *IEEE Trans. Intell. Transp. Syst.*, vol. 12, no. 4, pp. 942–953, Dec. 2011.

[11] J.-H. Kim and D.-S. Kum, "Threat prediction algorithm based on local path candidates and surrounding vehicle trajectory predictions for automated driving vehicles," in *Proc. IEEE Intell. Veh. Symp.*, Jul. 2015, pp. 1220–1225.

[12] J. Kim and D. Kum, "Collision risk assessment algorithm via lane-based probabilistic motion prediction of surrounding vehicles," *IEEE Trans. Intell. Transp. Syst.*, vol. 19, no. 9, pp. 2965–2976, Sep. 2018.

[13] R. Toledo-Moreo and M. A. Zamora-Izquierdo, "IMM-based lane-change prediction in highways with low-cost GPS/INS," *IEEE Trans. Intell. Transp. Syst.*, vol. 10, no. 1, pp. 180–185, Mar. 2009.

[14] D. Kasper, G. Weidl, T. Dang, G. Breuel, A. Tamke, A. Wedel, and W. Rosenstiel, "Object-oriented Bayesian networks for detection of lane change maneuvers," *IEEE Intell. Transp. Syst. Mag.*, vol. 4, no. 3, pp. 19–31, Fall 2012.

[15] M. Schreier, V. Willert, and J. Adamy, "An integrated approach to maneuver-based trajectory prediction and criticality assessment in arbitrary road environments," *IEEE Trans. Intell. Transp. Syst.*, vol. 17, no. 10, pp. 2751–2766, Oct. 2016.

[16] I.-H. Kim, J.-H. Bong, J. Park, and S. Park, "Prediction of driver's intention of lane change by augmenting sensor information using machine learning techniques," *Sensors*, vol. 17, no. 6, p. 1350, Jun. 2017.

[17] M. Bahram, C. Hubmann, A. Lawitzky, M. Aeberhard, and D. Wollherr, "A combined model- and learning-based framework for interaction-aware maneuver prediction," *IEEE Trans. Intell. Transp. Syst.*, vol. 17, no. 6, pp. 1538–1550, Jun. 2016.

[18] M. Bahram, A. Lawitzky, J. Friedrichs, M. Aeberhard, and D. Wollherr, "A game-theoretic approach to replanning-aware interactive scene prediction and planning," *IEEE Trans. Veh. Technol.*, vol. 65, no. 6, pp. 3981–3992, Jun. 2016.

[19] Y. Li, R. Yu, C. Shahabi, and Y. Liu, "Diffusion convolutional recurrent neural network: Data-driven traffic forecasting," 2017, *arXiv:1707.01926*.

[20] P. H. Phan, A. Q. Nguyen, L. D. Quach, and H. N. Tran, "Robust autonomous driving control using auto-encoder and end-to-end deep learning under rainy conditions," in *Proc. 8th Int. Conf. Intell. Inf. Technol.*, Feb. 2023, pp. 271–278.

[21] H. T. Ngoc, K. H. Nguyen, H. K. Hua, H. V. N. Nguyen, and L.-D. Quach, "Optimizing YOLO performance for traffic light detection and end-to-end steering control for autonomous vehicles in Gazebo-ROS2," *Int. J. Adv. Comput. Sci. Appl.*, vol. 14, no. 7, pp. 475–484, Jan. 2023.

[22] H. Gao, H. Su, Y. Cai, R. Wu, Z. Hao, Y. Xu, W. Wu, J. Wang, Z. Li, and Z. Kan, "Trajectory prediction of cyclist based on dynamic Bayesian network and long short-term memory model at unsignalized intersections," *Sci. China Inf. Sci.*, vol. 64, no. 7, Jul. 2021, Art. no. 172207.

[23] H. Wang, B. Lu, J. Li, T. Liu, Y. Xing, C. Lv, D. Cao, J. Li, J. Zhang, and E. Hashemi, "Risk assessment and mitigation in local path planning for autonomous vehicles with LSTM based predictive model," *IEEE Trans. Autom. Sci. Eng.*, vol. 19, no. 4, pp. 2738–2749, Oct. 2022.

[24] N. Deo and M. M. Trivedi, "Multi-modal trajectory prediction of surrounding vehicles with maneuver based LSTMs," in *Proc. IEEE Intell. Vehicles Symp. (IV)*, Jun. 2018, pp. 1179–1184.

[25] Z. Sheng, Y. Xu, S. Xue, and D. Li, "Graph-based spatial–temporal convolutional network for vehicle trajectory prediction in autonomous driving," *IEEE Trans. Intell. Transp. Syst.*, vol. 23, no. 10, pp. 17654–17665, Oct. 2022.

[26] S. Joerer, M. Segata, B. Bloessl, R. Lo Cigno, C. Sommer, and F. Dressler, "A vehicular networking perspective on estimating vehicle collision probability at intersections," *IEEE Trans. Veh. Technol.*, vol. 63, no. 4, pp. 1802–1812, May 2014.

[27] G. R. de Campos, A. H. Runarsson, F. Granum, P. Falcone, and K. Alenljung, "Collision avoidance at intersections: A probabilistic threat-assessment and decision-making system for safety interventions," in *Proc. 17th Int. IEEE Conf. Intell. Transp. Syst. (ITSC)*, Oct. 2014, pp. 649–654.

[28] B. Kim and K. Yi, "Probabilistic and holistic prediction of vehicle states using sensor fusion for application to integrated vehicle safety systems," *IEEE Trans. Intell. Transp. Syst.*, vol. 15, no. 5, pp. 2178–2190, Oct. 2014.

[29] A. Lambert, D. Gruyer, and G. Saint Pierre, "A fast Monte Carlo algorithm for collision probability estimation," in *Proc. 10th Int. Conf. Control, Autom., Robot. Vis.*, Dec. 2008, pp. 406–411.

[30] S. Ammoun and F. Nashashibi, "Real time trajectory prediction for collision risk estimation between vehicles," in *Proc. IEEE 5th Int. Conf. Intell. Comput. Commun. Process.*, Aug. 2009, pp. 417–422.

[31] A. Houénou, P. Bonnifait, and V. Cherfaoui, "Risk assessment for collision avoidance systems," in *Proc. 17th Int. IEEE Conf. Intell. Transp. Syst. (ITSC)*, Oct. 2014, pp. 386–391.

[32] K. Lee and H. Peng, "Evaluation of automotive forward collision warning and collision avoidance algorithms," *Vehicle Syst. Dyn.*, vol. 43, no. 10, pp. 735–751, Oct. 2005.

[33] Z. Gao, M. Bao, F. Gao, and M. Tang, "Probabilistic multi-modal expected trajectory prediction based on LSTM for autonomous driving," *Proc. Inst. Mech. Eng. D, J. Automobile Eng.*, vol. 238, no. 5, pp. 455–472, Apr. 2023.

[34] L. Tao, Y. Watanabe, Y. Li, S. Yamada, and H. Takada, "Collision risk assessment service for connected vehicles: Leveraging vehicular state and motion uncertainties," *IEEE Internet Things J.*, vol. 8, no. 14, pp. 11548–11560, Jul. 2021.

[35] B. Coifman and L. Li, "A critical evaluation of the next generation simulation (NGSIM) vehicle trajectory dataset," *Transp. Res. B, Methodol.*, vol. 105, pp. 362–377, Nov. 2017.

[36] R. Gray and D. Regan, "Accuracy of estimating time to collision using binocular and monocular information," *Vis. Res.*, vol. 38, no. 4, pp. 499–512, Feb. 1998.

[37] H. Chen, S. Feng, X. Pei, Z. Zhang, and D. Yao, "Dangerous driving behavior recognition and prevention using an autoregressive time-series model," *Tsinghua Sci. Technol.*, vol. 22, no. 6, pp. 682–690, Dec. 2017.

ZHENHAI GAO was born in Changchun, Jilin, China, in 1973. He received the Ph.D. degree in automotive engineering from Jilin University.

He is currently the Deputy Dean of Automotive Engineering and the Director of the State Key Laboratory of Automotive Simulation and Control Automotive Engineering, Jilin University. He has published more than 100 articles and authorized 20 invention patents. He is the coauthor of three books. His research interests include autopilot technology and human engineering.

Prof. Gao is a Distinguished Member of the Expert Committee Intelligent Connected Vehicle Innovation Alliance, the Chairperson of the Industrial Design Association in Jilin Province, and an Editorial Board Member of *International Journal of Human Factors Modelling and Simulation*.

MINGXI BAO was born in 1994. He received the master's degree from the College of Mechanical and Electrical Engineering, Shihezi University, Xinjiang, China, in 2017. He is currently pursuing the Ph.D. degree with the College of Automobile Engineering, Jilin University, Jilin, China. His current research interests include machine learning for trajectory prediction and decision-making of intelligent electric vehicles.

TAISONG CUI received the master's degree in vehicle engineering from Chongqing University, in 2009. He is currently the Head of Collision Safety with Chongqing Chang'an Automobile Company Ltd., where he oversees technical research in the safety domain and ensures the accomplishment of overall vehicle collision safety performance.

FANGYUAN SHI received the master's degree in vehicle engineering from Chongqing University, in 2010. Since 2011, he has been engaged in vehicle collision safety research and development with Chongqing Chang'an Automobile Company Ltd. His research interests include full-vehicle structural collision simulation, material fracture failure models, and battery mechanical impact safety. His current research focus is on collision risk prediction.

XIANQING CHEN received the master's degree in mechanical design and theory from Tianjin University, in June 2007. Since 2007, he has been involved in vehicle collision safety research and development with Chongqing Chang'an Automobile Company Ltd. His research interests include full-vehicle structural durability and characterization of material mechanical properties. His current research focus is on occupant protection control algorithms.

WENHAO WEN was born in 1997. He received the B.S. degree from the College of Automobile Engineering, Jilin University, Jilin, China, in 2019, where he is currently pursuing the Ph.D. degree. His current research interests include machine learning for path planning and control for intelligent electric vehicles and vehicle state estimation.

FEI GAO received the B.S. and Ph.D. degrees in automotive engineering from Jilin University, Changchun, China, in 2011 and 2017, respectively. From 2014 to 2015, she was a Visiting Student with the University of California at Berkeley, Berkeley, CA, USA. She is currently an Associate Professor with the State Key Laboratory of Automotive Simulation and Control Automotive Engineering, Jilin University. She is the coauthor of three books, more than 20 articles, and more than ten inventions. Her research interests include automotive human engineering and motion sickness.

RUI ZHAO (Member, IEEE) was born in Liaoyuan, Jilin, China, in 1986. She received the B.S. degree in computer science and technology from Northeast Normal University, in 2009, and the Ph.D. degree in computer science and technology from Jilin University, Changchun, China, in 2017.

She is currently an Associate Professor with the College of Automotive Engineering, Jilin University. She has authored about 30 journal articles and ten patents in China. She authored the monograph "Cyber Security Technology for Intelligent Automotive." Her research interests include cooperative control, functional safety, cybersecurity, and safety reinforcement learning for connected and automated vehicles.

Prof. Zhao is a member of the Society of Automotive Engineers.